Data-efficient methods applied to general spectral image capture

Mitchell R. Rosen, Francisco H. Imai, Mark D. Fairchild and Noboru Ohta

Munsell Color Science Laboratory
Chester F. Carlson Center for Imaging Science
Rochester Institute of Technology, Rochester, NY 14623 USA

(Received

Abstract

Commercialization of spectral imaging for color reproduction will require low bandwidth but highly accurate spectral image acquisition systems. *Self-adapting* systems are proposed as potential solutions. Such systems perform spectral content analysis on an encountered scene, reacting to the analysis by configuring efficient high quality spectral reconstruction. An experiment is reported comparing scene-derived spectral estimation transforms to static global transforms in multi-channel imaging simulations. For noise-free simulations, the adaptive approach showed clear benefit in terms of colorimetric and spectral statistics. When noise was added, the adaptive method continued to be superior in terms of spectral evaluations, but colorimetric degradation for the adaptive approach exceeded that of the static. This provided additional evidence that spectral reconstruction methods should reference psychometrics as an integral part of spectral error management.

Data-Efficient Methods Applied to General Spectral Image Capture

Mitchell R. Rosen, Francisco H. Imai, Mark D. Fairchild and Noboru Ohta
Munsell Color Science Laboratory
Chester F. Carlson Center for Imaging Science
Rochester Institute of Technology, USA

Introduction

Multi-channel visible spectrum imaging (MVSI) systems are under active investigation. There is growing anticipation that color reproduction will benefit from accurate pixel-level spectral estimates yielding higher quality output from more robust systems[1]. For simplicity MVSI is often called multispectral imaging, spectral imaging or multi-channel imaging.

Disadvantages to multi-channel spectral approaches are related to system complexity and the escalation in system throughput demand. Noise vulnerability is another critical issue. System designers will tradeoff these parameters to meet the demands of specific applications. To begin considering these tradeoffs, the universe of MVSI applications is divided into two categories. The first category is *limited* applications where only specific sorts of objects are imaged by a system. The class of potential objects can be pre-analyzed at the time of system design and the MVSI system can be streamlined to be efficient and yet give accurate results for those sorts of objects only. The second category of MVSI applications is *unconstrained* applications. This category is at disadvantage because there are no predetermined expectations for scene object spectral characteristics. Table I displays a chart of example applications and places them into one of these two major categories.

For *unconstrained* applications, highly precise spectral estimates will require a large number of spectrally distinct channels. Channels may have very narrow-band or wide-band spectral filtering. Even when properly tuned to avoid overwhelming noise, one needs to consider how to manage the large quantity of pixel-data that will be generated by the many channels.

The types of applications described as spectrally *limited* can enjoy the advantages of few spectrally wide-band channels. Thus, integration times may be lowered, illumination levels do not have to be as high, and imager sensitivity is not as critical. Relative to a many-channel *unconstrained* design, data throughput becomes far less of a problem and noise problems are reduced. When appropriate reconstruction methods are utilized these efficient systems can deliver high quality spectral estimates for objects from expected spectral classes[2-4].

Table II displays a comparison of the data demands for various configurations. As seen in Table II, full-frame three-channel 8-byte systems collect 18 mega-bytes for each 2K x 3K RGB image. If one were to increase the number of channels from 3 to 31 in order to create a general system for spectrally *unconstrained* applications, a single image would consist of nearly 200 mega-bytes prior to compression. For at least the earliest imaging stages, such an MVSI system would demand more than a 10 times increase in digital bandwidth over the three-band system. For digital video, the 1080p/60 format[5] is the current highest quality HDTV codified standard. It specifies 1080 lines by 1920 pixels progressively scanned at a refresh rate of 60 frames per second. While there are several manufacturers striving toward the goal[6], the e-cinema industry is struggling to build infrastructure that can handle the "prohibitive bandwidth requirements" of such

systems[7]. A 31 full-frame per channel multispectral system attempting to match the data flow requirements of 1080p/60 would need to transmit on the order of 4 giga-bytes per second through the system. Bit-depth of 10- or 12-bits would increase throughput demands accordingly. For comparison, Table II includes a 10-bit configuration for the high-end HDTV specification.

Others have suggested that a solution to the data crunch of general MVSI systems is to immediately compress the data[1]. Here a compression stage introduced prior to image file storage will reduce the amount of data the system eventually carries. A number of compression schemes for visible-spectrum multi-channel images have been considered[8-11]. While it is certain that fast, efficient hardware could eventually be built to move, process, encode and compress images from general high-quality high-speed many-channel MVSI systems, such as those in the right two columns of Table II, the question remains: will such hardware be built and at what cost? It will hurt the acceptance of spectral reproduction if excessive dataflow demands are considered integral to system requirements.

Hardeberg provides an extensive list of conclusions from various worldwide research groups for the number of channels necessary for high quality spectral estimation[12]. Some of the groups listed are primarily interested in *limited* applications based on specific classes of spectral objects, such as fine arts paintings. Most of these groups find that seven or fewer channels are sufficient for *limited* applications.

Since a scene can be thought of as consisting of a limited number of spectrally distinct object, Hardeberg's list leads to the argument that most individual scenes should be accurately spectrally imaged by an MVSI system with seven or fewer channels.

Unfortunately, a different MVSI system might be needed to be customized for each scene. The self-adapting systems discussed below do just that: they tailor themselves to the spectral constituencies of the environment in order to deliver only a few channels of data and a transform which allows high quality spectral reconstruction. Thus, these are data-efficient system for *unconstrained* MVSI applications.

Self-adapting MVSI Proposal

A hybrid approach to MVSI is proposed. Like systems designed for *limited* applications, these devices will be data-efficient because they will only deliver a few channels coming from wideband filtering. Like systems designed for *unconstrained* applications, high quality spectral estimates will be expected. The solution is based on a capability for scene analysis that derives for each scene an updated transformation to spectral estimates based upon a sampling of scene spectra. Some systems will take advantage of this analysis stage to modigy their channel filtering in reaction to scene spectral content.

Conceptually, there are two subsystems in a self-adapting MVSI system. The first subsystem consists of a general system capable of gathering highly accurate spectral information about any potential scene spectra. The second subsystem is an adaptive low-data-bandwidth system. Some system designs might not physically separate the two subsystems. They may, in fact, work with the same optics, the same imager, maybe even the same filters. On the other hand, there may be very good reasons to physically separate the two subsystems. In that case, it is likely that the general subsystem will be ancillary to the tailorable subsystem, and thus may be low in spatial and possibly

temporal resolution. It may also be low quality in other ways, because it is used only for analysis and will not be used to capture final images. The tailorable subsystem will be the main system through which the scene is eventually captured.

Figure 1 shows a summary of self-adapting data-efficient systems. In Step 1, the scene, or a portion of the scene, is imaged by the system at high spectral resolution but low spatial resolution, producing $S_g(x,y,\lambda)$. For some systems, $S_g(x,y,\lambda)$ will be collected through a specialized secondary imaging sub-system. Other systems will not have the luxury of having two imaging sub-systems and will perform this data acquisition through the main system.

Step 2 is the central aspect of the self-adapting system. An analysis of $S_g(x,y,\lambda)$ is accomplished. This analysis is used to tailor the system to the spectral characteristics of the scene. Those systems that are configurable continue to Step 3 where channel filterings are chosen or synthesized based upon the discoveries of the Step 2 analysis. All systems then proceed to Step 4 where the Step 2 analysis is used to derive a mathematical transform, $f_t()$, from channel digits to spectral estimates.

High spatial resolution images of the scene are taken in Step 6, yielding $M_{dc}(x,y,i)$ where i spans from 1 to number of channels being used. $f_t()$ and $M_{dc}(x,y,i)$ are stored for future use. Subsequently, transform $f_t()$ may be used to reconstruct spectra such that $S_t(x,y,\lambda)=f_t(M_{dc}(x,y,i))$. Since the system is self-adapting, it will react to new scenes by repeating Steps 1 through 6, so that as the spectral character of scene contents change, new system configurations and transforms will follow.

Experimental Design – Testing Self-adaptive Systems

Experiments were designed to test the value of the scene-based transform derivation as found in Step 4 of Figure 1. These experiments are important for evaluation of the self-adapting system concept, and will provide additional data for use in the continuing debate over the spectral dimensionality of object colors as outlined by Hardeberg[12] and on the feasibility of universal spectral characterization targets as called for by Imai, et al.[13], among others.

The channel spectral sensitivities of a set of simplistic multi-channel camera systems, with 3, 6, 9 or 31 channels, were specified within a MATLAB simulation environment. Channel spectral band-pass widths ranged from from infinitely-narrow to 150nm for full width at half maximum (FWHM) height. Spline routines were used to create gaussian-like spectral profiles for the channels. Peak wavelengths were equally spaced to the closest integer multiple of 10nm throughout the visible range for each set of channels. Figures 2 through 5 show examples channel sets with a selection of channel counts and band-pass widths.

Figure 6 illustrates the logic flow of the experiment, with details of blocks 1 through 4 found in Figures 7 through 10, respectively. For each experiment, two systems were simulated: one *static* and one *self-adaptive*. The significant difference between these two system simulations was the method used to derive the transform from digital counts to reflectance estimates.

The *static* system is shown in block 2 of Figure 6 and detailed in Figure 8. This approach is similar to current MVSI systems where a spectral reconstruction transform is derived as a characterization step rather than as part of the scene capture mechanism of

the system. *Static* systems do not have the ability to self-adapt. Thus, a single transformation, M, was derived within block 2's Global Setup and that single transformation was used within every iteration of the Iterative Scene Imaging to estimate spectra.

A second simulated system was *self-adapting* as shown in block 3 of Figure 6 and detailed in Figure 9. Within the simulation's Iterative Scene Imaging, this system practices the proposed capability to analyze the spectra of a scene to derive a custom transform, M^s.

In both Figure 6's block 2 and block 3, there is Iterative Scene Imaging. For each simulated system, the Iterative Scene Imaging is where spectra are selected at random from a database, imaged and then reconstructed. 20 spectra are selected from the database for every iteration. In block 4, detailed in Figure 10, statistics associated with the two simulated systems were averaged over 100 iterations and compared.

Two spectral reflectance databases were used in this study. The first was a collection of human face reflectances measured by Sun for use in his spectral portraiture investigations[14-16]. The set consisted of 544 samples, 16 measurements from each of 34 individuals. The Sun database contains samples taken from the following parts of the human face:

- facial skin
- hair
- iris
- lips

Subjects came from the following racial groups:

- Pacific-Asian
- Caucasian
- Black
- Subcontinental-Asian
- Hispanic

A second spectral reflectance database that also included human skin and hair, as Sun's did, but in addition a large selection of other natural objects is the Vrhel natural object reflectance dataset[17]. It consisted of the measurement of 170 objects including the following:

- rocks, soil and sand
- leaves, grass, flowers, bark and wood
- fruit, nuts, seeds, sugar, vegetables, corn, gum, bread and pancake
- asphalt
- textiles
- plastics
- leather
- human skin and hair:

  Caucasian

  East Indian

  African American

  Asian

In all cases, the illuminant under which the object spectra were "captured" within the Iterative Scene Imaging of blocks 2 and 3 was based on the measurement of a

GretagMacbeth light booth painted tungsten daylight simulator with a correlated color temperature of 7279K. Throughout the experiments, spectra consisted of 31 samples between 400nm and 700nm in 10nm increments.

The search for robust error statistics for describing the quality of a spectral match is a current line of active research[18]. There were three error metrics chosen for analysis in this experiment. These were average RMS, EMASE and average ΔE^*_{ab} between colorimetry calculated for the 2º standard observer under D65. Each, discussed below, is relevant to describing aspects of spectral mismatch.

From a color reproduction standpoint, the most familiar of the performance metrics is ΔE^*_{ab}. ΔE^*_{ab} depends upon values which are related to spectra in that they are an integration step away from reflectance after a specific illuminant has been imposed. The metric is, thus, an indirect spectral evaluation method as it cannot differentiate among various spectra that integrate to the same colorimetry. It is also highly dependent on the illuminant used. Although these drawbacks are significant, it would be folly to ignore the importance of metrics that are based on visual validity as ΔE^*_{ab} is. This has been well understood for many years as evidenced by at least 40 years of search for a robust metamerism index[19], a method for combining colorimetric and spectral error.

RMS is a typical metric used for describing the error between an original and a reconstructed spectrum. It is useful for measuring the full breath of a spectral mismatch. Every error throughout the spectrum participates in building the value. The squaring operation gives a non-linear increase in penalty to larger errors. Its advantage is that it can easily be used to create an interval scale to compare spectral reconstructions. Intuition is challenged, though, when attempting to assign tolerances to RMS values.

Maximum absolute spectral error, here called MASE, is occasionally used to describe spectral reproduction quality. At each sample point across the wavelengths of interest, a spectrum and its reconstruction are compared. This produces the individual maximum absolute spectral error, IMASE. The largest IMASE from a set of spectra is reported as the MASE. In isolation, MASE cannot be considered to be very informative with respect to performance of a spectral estimation task since it only describes error on a single wavelength of a single spectrum from a set. But, averaging MASE over a large number of iterations where a different set of random spectra, the comparison set, are chosen from the spectral database for each iteration, creates a more useful statistic. EMASE, the expected maximum absolute spectral error, is this new statistic. As long as the number of spectra comprising each comparison set is much smaller than the size of the database but large enough, on average, to share the statistics of the full database, it is not possible for EMASE to be heavily skewed by unusual individual spectra and does produce a meaningful performance measure.

Three basic experiments were implemented. Tables III to V describe, respectively, the parameters to Experiments 1 to 3. Experiment 1 synthesized noiseless channels for imaging the Sun human face database. Experiment 2 was also a noiseless system and uses the Vrhel natural objects database. Experiment 3 introduced noise and with it the Vrhel database is used.

Results and Discussion

6 eigenvectors were chosen after PCA analysis for linear reconstruction of spectra from channel digital counts. For the Sun database, 6 eigenvectors represented 99.9921%

of the database variance. For the Vrhel database, a different set of 6 eigenvectors represented 99.9492% of the database variance. Static systems derived their eigenvector reconstruction matrices by analyzing the full databases (Global Setup of Figure 8). Self-adapting systems derived their reconstruction matrices only on scene contents (Scene-specific Setup of Figure 9).

As expected, the self-adapting approach improves upon the static approach in Experiments 1 and 2, for all statistics, for both databases and for all system configurations. The simulated systems for these experiments were all free from any noise. Table VI illustrates for each statistic the average percent improvement from static to self-adapting for these experiments.

For the pure spectral statistics, RMS and EMASE, the 31-channel systems represent the high quality asymptote. Figures 11 and 12 show spectral evaluation results for the Vrhel database. For this database, the 9-channel systems reach the 31-channel asymptote at FWHM sensitivity band-pass widths of between approximately 40nm and 100nm. This is true in both the static implementations and the self-adapting ones. 6-channel systems also show the tendency to reduce error as sensitivity band-pass goes from infinitely-narrow toward mid-widths between approximately 50nm and 130nm and then error increases as the band-widths become very wide. Results for the RMS and EMASE statistics of the Sun database are very similar.

Ohta, in 1981, concluded that spectral band-pass of the channel sensitivities "only slightly influenced" the quality of spectral reconstruction results.[20]. His experiment simulated a series of 6-channel systems with sensitivity band-pass widths that ranged from approximately 30nm to 90nm FWHM. The spectral database he used for simulated

capture was the 24 colors from a Macbeth Color Checker color rendition chart. Figures 11 and 12 show very low bandwidths and very high bandwidths to deliver substantially higher spectral error. Ohta's previous experiment only tested a comparatively limited range of bandwidths and would likely have seen the larger negative influence of channel width had he extended his inquiry.

Figures 11 and 12 show error to increase for the channel spectral sensitivity shapes at the extremes. Although in all cases, regardless of channel width, many potential spectral shapes can be confused by a system with only 6 channels, given the fact that the spectra we are considering are relatively smooth and somewhat consistent, optimal channel sampling width will lower average errors. For very narrow sensitivities, the spectral features of the reflectances are undersampled making it likely that many are completely missed. Conversely, as bandwidths become very wide, spectral features across the spectrum are highly convolved making it difficult to separate where they begin and where they end. In the limiting case where channel sensitivities are flat across the spectrum, it is completely impossible to separate spectral features.

Colorimetric error results for both the Vrhel and Sun databases can be seen in Figures 13 and 14. Much of these ΔE^*_{ab} results did not follow the pattern shown by the spectral statistics in Figures 11 and 12. Although the very low bandwidths show the 6-, 9- and 31-channel systems holding their usual order of 31-channels highest quality then 9- and then 6-, at higher band-passes there are crossovers creating reversal of this trend for all but the Sun static implementation. For spectral sensitivity widths greater than the crossover bandwidths, it is the 6-channel systems that have the lowest average ΔE^*_{ab}.

Even for the Sun static example, as seen in Figure 14, the advantage of having more than 6 channels is diminished as spectral sensitivity bandwidths approach 110nm.

As explained under Experiment Design, the method for deriving a reconstruction transform from channel values was matrix synthesis based on PCA decomposition of the spectra. The spectra training set consisted of the full database for the static implementations and of a selection from the full database for the self-adapting implementations. There was no colorimetric or visual component to this analysis. Since the transform was built solely from a spectral perspective, it is satisfying that a 31-channel approach always does better than its 9-channel counterpart and, in turn, they are both always superior to a 6-channel scheme in terms of spectral metrics. Colorimetry, when not under control of the transform building algorithm, has the ability to defy expectations, as it has here.

A closer look was taken of the 10nm and 100nm channel bandwidth static implementation for 6- and 9-channels Vrhel database examples. Each of the individual 170 Vrhel samples was examined. For the 10nm bandwidth example, 86% of the samples in the 9-channel simulation had superior RMS scores compared to the same samples in the 6-channel simulation and 61% of the 9-channel individual samples had lower ΔE^*_{ab}. For the 100nm bandwidth case, the percent of 9-channel samples with better average RMS error increases to 98% but ΔE^*_{ab} superiority falls to 35%. These findings are consistent with the trends seen in Figure 11 - 13. Figures 15 and 16 show four individual spectra from the Vrhel database and their reconstructions from the 6- and 9-channel 100nm channel bandwidth system. Relative to the 6-channel curves, the 9-

channel reconstructed curves in these figures all have lower RMS error and IMASE while the 6-channel curves all have superior colorimetric performance.

The average spectral error profiles for the 6- and 9-channel 100nm systems is collected and presented in Figure 17. The differences appear small. Summing the averages shows the 9-channel system to have a slight average error advantage. It is only after weighting the averages by multiplying by the 2 degree color matching functions that the 6-channel system is shown to have a significant advantage particularly with respect to ΔX performance. The x-bar weighted average error is 2/10% better for the 6-channel 100nm band-pass system than it is for the 9-channel system. The 6-channel system also enjoys better y-bar weighted results while the 9-channel system shows advantage in z-bar weighted error, but these differences are an order of magnitude below the 6-channel's x-bar weighted error advantage. Using the average ΔXYZ results (under equal energy illuminant) and adding it to an 18% neutral, the 6-channel system would derive a color which has 0.13 less ΔE^*_{ab} from the original than the 9-channel system would.

To check the impact of illuminant on these phenomena, the individual sample analysis was performed a second time after imposing Illuminant A on the reconstructed spectra. The trends remained intact for Illuminant A. Spectral database can also be ruled out as a cause of this finding since, as shown by comparing Figures 13 and 14, a change in spectral database has little effect on results.

Two factors remain likely suspects for causing the aberration. One is the center wavelength and shape of the channel band-passes. The second is the method in which the channel-to-spectrum transform is generated. System designers may or may not be able to specify filter center wavelengths and their spectral shape, but they will definitely have the

ability to specify how transforms are derived. Thus, in addition to being an interesting set of observations, this turn of events carries with it an important reminder. Transform building methods must not be so naïve as to allow colorimetric results to go in the wrong direction. As colorimetry is illuminant-based, one needs to exert caution in its use within spectral reconstruction systems, but it must be recognized that many spectra can produce the same amount of spectral error, so the use of vision-based metrics to guide how to manage spectral error is fully appropriate.

The experimental design for Experiment 3 was similar to that for Experiment 2 except only the 6- and 9-channel systems were analyzed and white noise was added to the systems. Like Experiment 2, the Vrhel database was used. Table VII displays the average percent change from static to self-adapting for Experiment 3. Figures 18 through 20 show the full Experiment 3 results and include the 6- and 9-channel Experiment 2 results for comparison purposes.

Like earlier results, the self-adaptive systems improve upon the static systems for all the purely spectral statistics, RMS and EMASE, as shown in Figures 18 and 19. Consistent with a phenomenon noted above, spectral statistics were not necessarily representative of colorimetric statistics. Figure 20 shows that with respect to ΔE^*_{ab}, for most widths, the noisy static system was actually superior to the self-adapting system. The consistency of the colorimetric loss for self-adaptive systems flies in the face of intuition.

The introduction of noise for Experiment 3 is actually to the relative advantage of the static systems. Static systems for the Vrhel database are based upon PCA analysis of 170 spectra. Each individual iteration of the self-adaptive simulation is based upon PCA

analysis of 20 spectra. When the measurement of the spectra is noisy, then averaging over 170 samples will reduce the effect of noise relative to averaging over 20 samples. Regardless of the negative influence of noise, the self-adaptive system continues to enjoy the advantage of having a reconstruction matrix tailored to the specific scene spectra. As shown in Figures 18 and 19 the amount of noise added to the system did not overwhelm the spectral superiority of the self-adaptive system. As discussed above, once again, the fact that colorimetry was not consulted when building the transforms resulted in unfortunate error manifestation. The conclusion becomes stronger that such naïve approaches to building transforms must be addressed.

Conclusions

Data-efficient self-adaptive systems are proposed as a potential answer to the need to reduce data throughput demands for multi-channel systems for color reproduction. These systems include an analysis stage for deriving a scene-dependent transform from system digital counts to spectral estimates. Some systems may also have a channel selection or synthesis stage.

A series of three experiments were carried out to evaluate the value of the scene analysis stage of these systems. Two different spectral databases were used: Sun's human face reflectance database and Vrhel's natural objects reflectance database. It was determined that systems with 3, 6, 9 and 31 channels all enjoy benefit in their spectral reconstruction from self-adaptive behavior. This was true for simulations with and without noise. When noise was introduced to the simulations the spectral statistics continued to show self-adaptation improvements.

Surprising results included that fact that for these simulations, wide-band 6-channel systems were able to demonstrate lowest colorimetric error for many configurations although the spectral statistics favored the 9- and 31-channel approaches. Similarly, after noise was added self-adapting approaches improved spectral reconstruction but were not always colorimetrically superior under these conditions. These were important reminders that when spectral reproduction is not perfect, reduction of spectral error alone is not sufficient to ensure best color reproduction.

Future investigations will include research on the topic of improved transformation derivation. Colorimetry or related psychometrics will be incorporated for spectral error management during the construction process for channel-to-spectrum transforms. Also, additional features such as channel selection and channel synthesis in configurable self-adaptive systems will be explored.

Acknowledgements

The authors would like to acknowledge the Display Technology Laboratories of Sony Corporation for their support of this research.

References

[1]B. Hill, (R)evolution of Color Imaging Systems, *Proceedings of the First European Conference on Color in Graphics*, Imaging and Vision, 473-479 (2002).

[2]S. Park and F. Huck, Estimation of spectral reflectance curves from multispectral image data, *Applied Optics*, **16** 3107-3114 (1977).

[3]T. Shiobara, S. Zhou, H. Haneishi, N. Tsumura, and Y. Miyake, Improved Color Reproduction of Electronic Endoscopes, *J. Imaging Sci. Technol.* **40** 494-501 (1996).

[4]F. H. Imai and R. S. Berns, Spectral Estimation Using Trichromatic Digital Cameras, *Proceedings of the International Symposium on Multispectral Imaging and Color Reproduction for Digital Archives*, 42-49 (1999).

[5]Society of Motion Pictures and Television Engineers, SMPTE Standard for Television-1920x1080 Scanning and Analog and Parallel Digital Interfaces for Multiple-Picture Rates, *SMPTE 274M-1998*, SMPTE, White Plains, N.Y. (1998).

[6]S. Wiedemann, 24/P HDTV: The Fall of Film Production, client.henninger.com/pickup/arlington/Engineering/hdtvfilm24.doc (2001).

[7]R. Corrigan, B. Lang, D.LeHoty, and P.Alioshin, An Alternative Architecture for High Performance Display, *SMPTE Journal*, **109** (2000).

[8]T. Keusen, Multispectral color system with an encoding format compatible with the conventional tristimulus model, *J. Imaging Sci. Technol.* **40**, 510-515 (1996).

[9]W. Kondou, K. Miyata, H. Haneishi and Y. Miyake, An Evaluation of Image Quality for Compressed Multi-spectral Image, *Proceedings of the International Symposium on Multispectral Imaging and Color Reproduction for Digital Archives*, 143-146 (1999).

[10]M. Hauta-Kasari, J. Lehtonen, J. Parkkinen and T. Jaaskelainen, Spectral image compression for data communications, *Proceedings of the SPIE* **4300**, 42-49 (2001).

[11]N. Matsushiro, F. Imai and N. Ohta, Principal Component Analysis of Spectral Images Based on the Independence of the Color Matching Function Vectors, *Proceedings of the Third International Conference on Multispectral Color Science*, 77-80 (2001).

[12]J. Hardeberg, On the spectral dimensionality of object colors, *Proceedings of the First European Conference on Color in Graphics, Imaging and Vision*, 480-485 (2002).

[13]F. Imai and R. Berns, Spectral Estimation of Artist Oil Paints using Multi-filter Trichromatic Imaging, *Proceedings of SPIE* **4421**, 504-507 (2002).

[14]Q. Sun and M. Fairchild, Statistical Characterization of Spectral Reflectances in Spectral Imaging of Human Portraiture, *Proceedings of IS&T/SID Ninth Color Imaging Conference*, 73-79 (2001).

[15]Q. Sun and M. Fairchild, A New Procedure for Capturing Spectral Images of Human Portraiture, *Proceedings of SPIE* **4421**, 496-499 (2002).

[16]Available at www.cis.rit.edu/mcsl/online/lippmann2000.shtml. Follow the link to spectral measurement databases.

[17]M. Vrhel, R. Gershon and L. Iwan, Measurement and analysis of object reflectance spectra, *Color Research and Applications,* **19**, 4-9 (1994).

[18]F. H. Imai, M. R, Rosen, R. S. Berns, Comparative Study of Metrics for Spectral Match Quality, *Proceedings of the First European Conference on Color in Graphics, Imaging and Vision*, 492-496 (2002).

[19]I. Nimeroff and J. Yurow, Degree of Metamerism, *J. Opt. Soc. Am.* **55**, 185-190 (1965).

[20]N. Ohta, Maximum errors in estimating spectral-reflectance curves from multispectral image data, *J. Opt. Soc. Am. Letters*, **71**, 910-913 (1981).

Table I. “Unconstrained” and “limited” spectral imaging applications. In general, the categories on the left require apparatuses that can handle scene objects with arbitrary spectra whereas categories on the right can rely on devices tailored to predetermined spectral characteristics of expected scene objects. Placements are for illustration only as there will be specific instances where applications may switch columns.

Table II. Data demands prior to compression or encoding created by full frame per channel image capture for various applications. The two right columns represent the volume of data that would be generated, respectively, for 16 or 31 multi-channel implementations.

Table III. Parameters to Experiment 1.

Table IV. Parameters to Experiment 2.

Table V. Parameters to Experiment 3.

Table VI. Experiments 1 and 2 percent average improvements from static to self-adapting systems.

Table VII. Experiment 3 percent average change from static to self-adapting systems.

Figure 1. Self-adapting data-efficient spectral acquisition.

Figure 2. Example of 3-channel system with FWHM spectral band-pass of 30nm.

Figure 3. Example of 6-channel system with FWHM spectral band-pass of 100nm.

Figure 4. Example of 9-channel system with infinitely-narrow spectral band-pass.

Figure 5. Example of 31-channel system with FWHM spectral band-pass of 60nm.

Figure 7. Common Setup. Block 1 from Figure 13.

Figure 8. Static System Simulation. Block 2 from Figure 13. pinv() is the pseudo-inverse operator. MASE is maximum absolute spectral error.

Figure 9. Self-adaptive System. Block 3 from Figure 13. pinv() is the pseudo-inverse operator. MASE is maximum absolute spectral error.

Figure 10. Analysis. Block 4 from Figure 13.

Figure 11. RMS for Experiments 1 and 2 considering 6-, 9- and 31-channel systems imaging the Vrhel database.

Figure 12. EMASE for Experiments 1 and 2 considering 6-, 9- and 31-channel systems imaging the Vrhel database.

Figure 13. ΔE^*_{ab}, for experiment 1 and 2 considering 6-, 9- and 31-channel systems imaging the Vrhel database.

Figure 14. ΔE^*_{ab}, for experiment 1 and 2 considering 6-, 9- and 31-channel systems imaging the Sun database.

Figure 15. Samples 15, 16 and 17 from the Vrhel natural objects database and their 6-channel and 9-channel system reconstructions for the 100nm-wide channel spectral sensitivity width.

Figure 16. Sample 73 from the Vrhel natural objects database and its 6-channel and 9-channel system reconstruction for the 100nm-wide channel spectral sensitivity width.

Figure 17. Spectral error profiles for the 6-channel and 9-channel 100nm-wide channel spectral sensitivity width systems.

Figure 18. RMS results of Experiment 3 (1% noise) compared to Experiment 2 (noiseless). All are of the Vrhel database. Key: Open squares = 1% noise, static; open circles = 1% noise, self-adapting; diamonds = noiseless, static; X's = noiseless, self-adapting.

Figure 19. EMASE results of Experiment 3 (1% noise) compared to Experiment 2 (noiseless). All are of the Vrhel database. Key: Open squares = 1% noise, static; open circles = 1% noise, self-adapting; diamonds = noiseless, static; X's = noiseless, self-adapting.

Figure 20. ΔE^*_{ab} results of Experiment 3 (1% noise) compared to Experiment 2 (noiseless). All are of the Vrhel database. Key: Open squares = 1% noise, static; open circles = 1% noise, self-adapting; diamonds = noiseless, static; X's = noiseless, self-adapting.

Spectrally Unconstrained Applications	Spectrally Limited Applications
• snap shots	• bio-medical imaging/telemedicine
• commercial photography	• fine arts reproduction and conservation
• video:	• color-critical industrial communication:
entertainment	graphic arts
special effects	textiles
conferencing	agriculture
• remote sensing	• machine vision
• astronomy	• cosmetics

Table I

Application Image Specs	Traditional 3 Channel Uncompressed Unencoded	16 Channel Uncompressed Unencoded	31 Channel Uncompressed Unencoded
Commercial studio 2K x 3K 8bits / pixel	18 Mb / image	96 Mb / image	186 Mb / image
720p/24 HDTV 720 x 1280 x 24Hz progressive scan 8bits / pixel	63 Mb / second	338 Mb / second	654 Mb / second
1080p/60 HDTV 1080 x 1920 x 60Hz progressive scan 8bits / pixel	356 Mb / second	1.9 GB / second	3.7 GB / second
1080p/60 HDTV 1080 x 1920 x 60Hz progressive scan 10bits / pixel	445 Mb / second	2.4 GB / second	5.6 GB / second

Table II

Experiment 1 – perfect system (human face reflectances)	
experimental parameter	**values**
Spectral Database	Sun human face reflectances
Number of Channels	3,6,9 and 31
Channel spectral sensitivity band-pass	infinitely-narrow; 10nm to 150nm in steps of 10nm
Noise level	none

Table III

Experiment 2 – perfect system (natural objects reflectances)	
experimental parameter	**values**
Spectral Database	Vrhel natural objects reflectances
Number of Channels	3,6,9 and 31
Channel spectral sensitivity band-pass	infinitely-narrow; 10nm to 150nm in steps of 10nm
Noise level	none

Table IV

Experiment 3 – noisy system (natural objects reflectances)	
experimental parameter	**values**
Spectral Database	Vrhel natural objects reflectances
Number of Channels	6 and 9
Channel spectral sensitivity band-pass	infinitely-narrow; 10nm to 150nm in steps of 10nm
Noise level	white noise, mean of 0, standard deviation of .01

Table V

Experiments 1 and 2: Static to Self-Adaptive Comparison Over All Channel Widths			
statistic	# channels	Exp. 1 Improvement	Exp. 2 Improvement
RMS	3	9.54%	11.33%
	6	20.41%	20.24%
	9	20.15%	21.61%
	31	19.59%	21.67%
EMASE	3	9.67%	12.63%
	6	22.42%	20.09%
	9	24.44%	19.13%
	31	25.00%	18.52%
ΔE^*_{ab}	3	5.13%	7.03%
	6	17.55%	16.99%
	9	0.58%	23.45%
	31	1.70%	22.52%

Table VI

Experiment 3: Static to Self-adaptive Comparison Over All Channel Widths		
statistic	# channels	Average improvement
RMS	6	9.87%
	9	7.05%
EMASE	6	11.48%
	9	7.39%
ΔE^*_{ab}	6	-3.71%
	9	-10.90%

Table VII

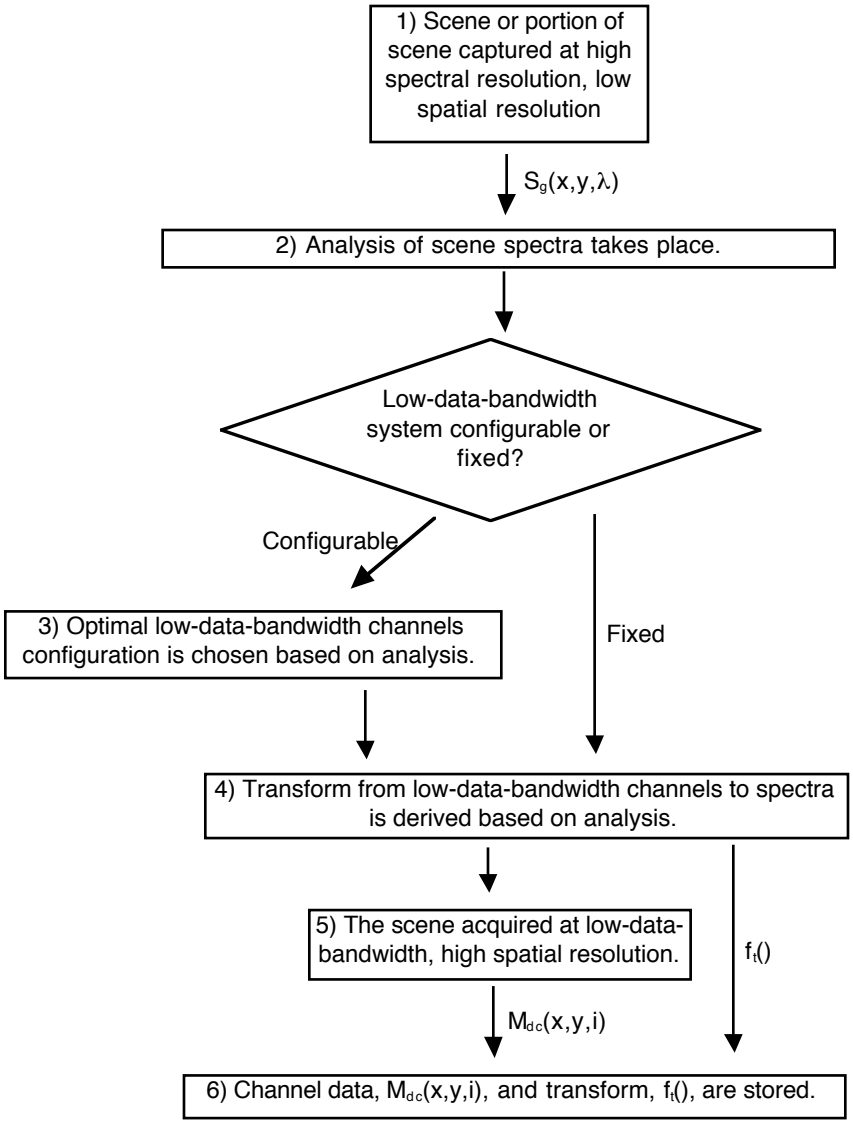
1) Scene or portion of scene captured at high spectral resolution, low spatial resolution
$S_g(x,y,\lambda)$
2) Analysis of scene spectra takes place.
Low-data-bandwidth system configurable or fixed?
Configurable
Fixed
3) Optimal low-data-bandwidth channels configuration is chosen based on analysis.
4) Transform from low-data-bandwidth channels to spectra is derived based on analysis.
5) The scene acquired at low-data-bandwidth, high spatial resolution.
$f_t()$
$M_{dc}(x,y,i)$
6) Channel data, $M_{dc}(x,y,i)$, and transform, $f_t()$, are stored.

Figure 1

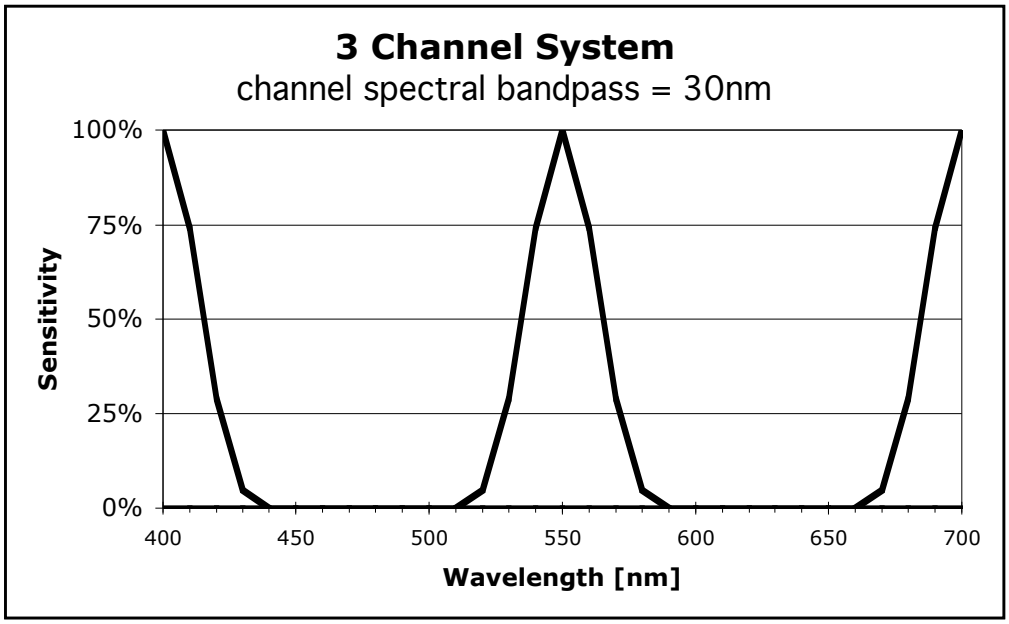
3 Channel System
channel spectral bandpass = 30nm
100%
75%
50%
25%
0%
Sensitivity
400
450
500
550
600
650
700
Wavelength [nm]

Figure 2

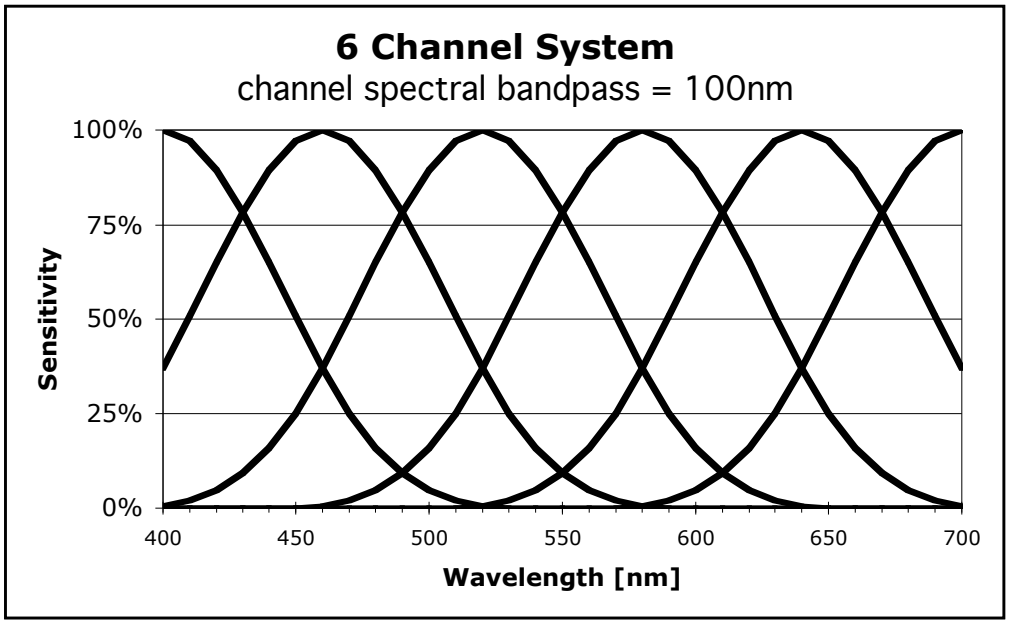
6 Channel System
channel spectral bandpass = 100nm
100%
75%
50%
25%
0%
Sensitivity
400
450
500
550
600
650
700
Wavelength [nm]

Figure 3

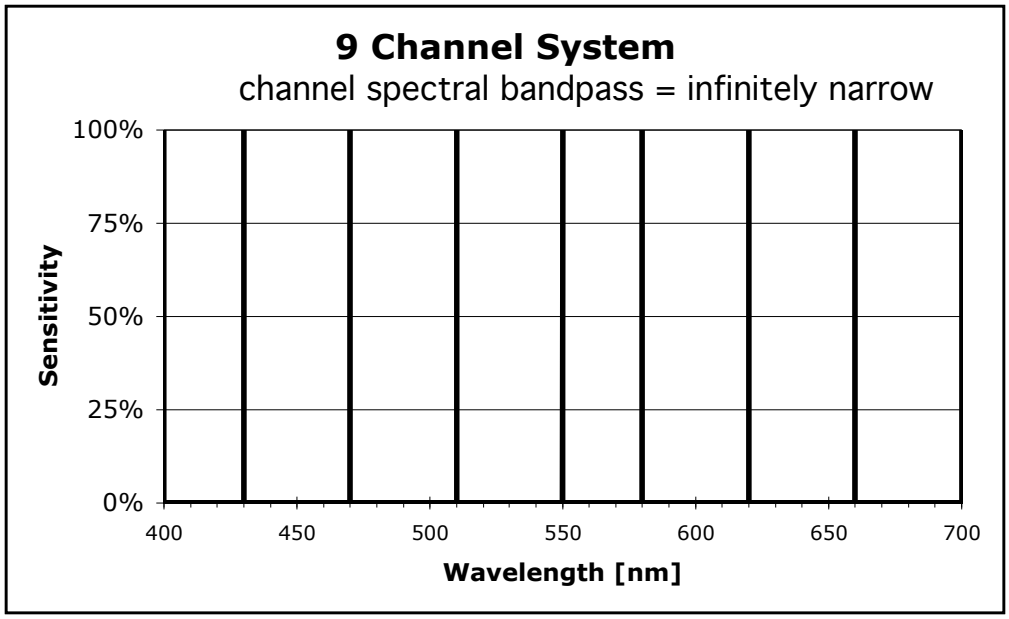
9 Channel System
channel spectral bandpass = infinitely narrow
100%
75%
50%
25%
0%
Sensitivity
400
450
500
550
600
650
700
Wavelength [nm]

Figure 4

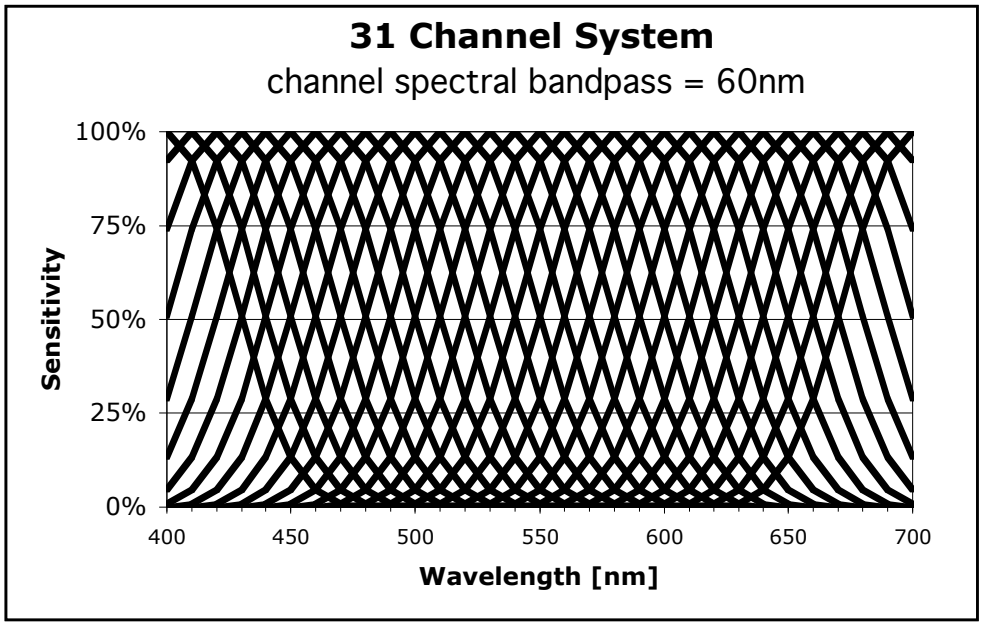
31 Channel System
channel spectral bandpass = 60nm
100%
75%
50%
25%
0%
Sensitivity
400
450
500
550
600
650
700
Wavelength [nm]

Figure 5

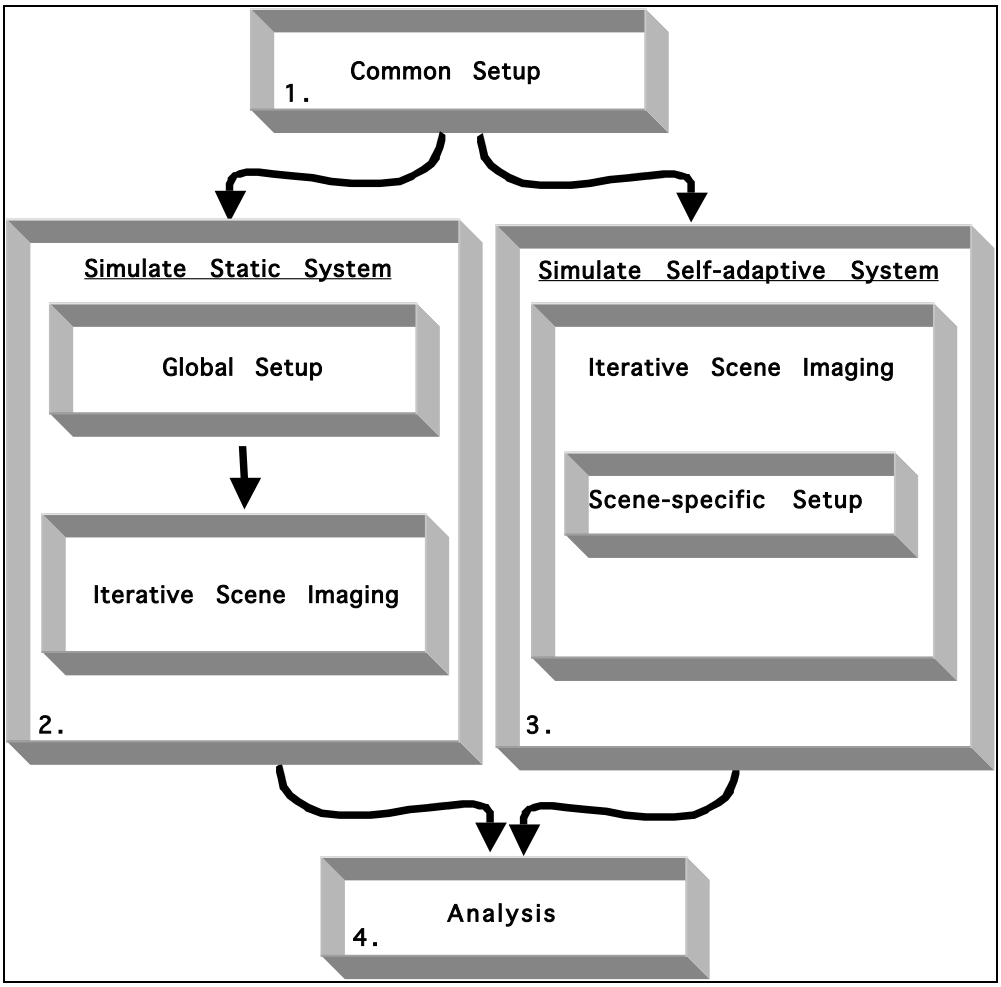
Common Setup
1.
Simulate Static System
Global Setup
Iterative Scene Imaging
2.
Simulate Self-adaptive System
Iterative Scene Imaging
Scene-specific Setup
3.
Analysis
4.

Figure 6

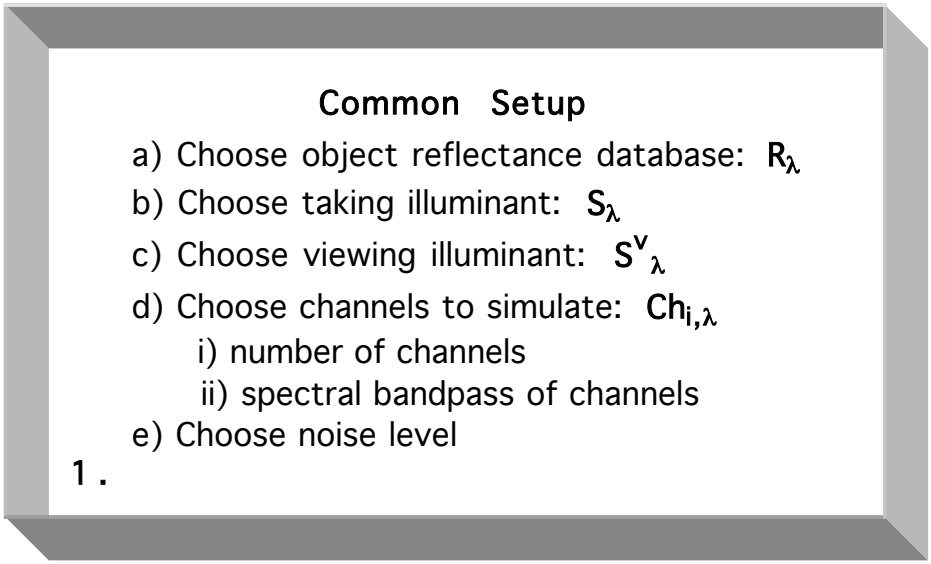
Common Setup
a) Choose object reflectance database: R_λ
b) Choose taking illuminant: S_λ
c) Choose viewing illuminant: S^v_λ
d) Choose channels to simulate: $Ch_{i,\lambda}$
i) number of channels
ii) spectral bandpass of channels
e) Choose noise level
1 .

Figure 7

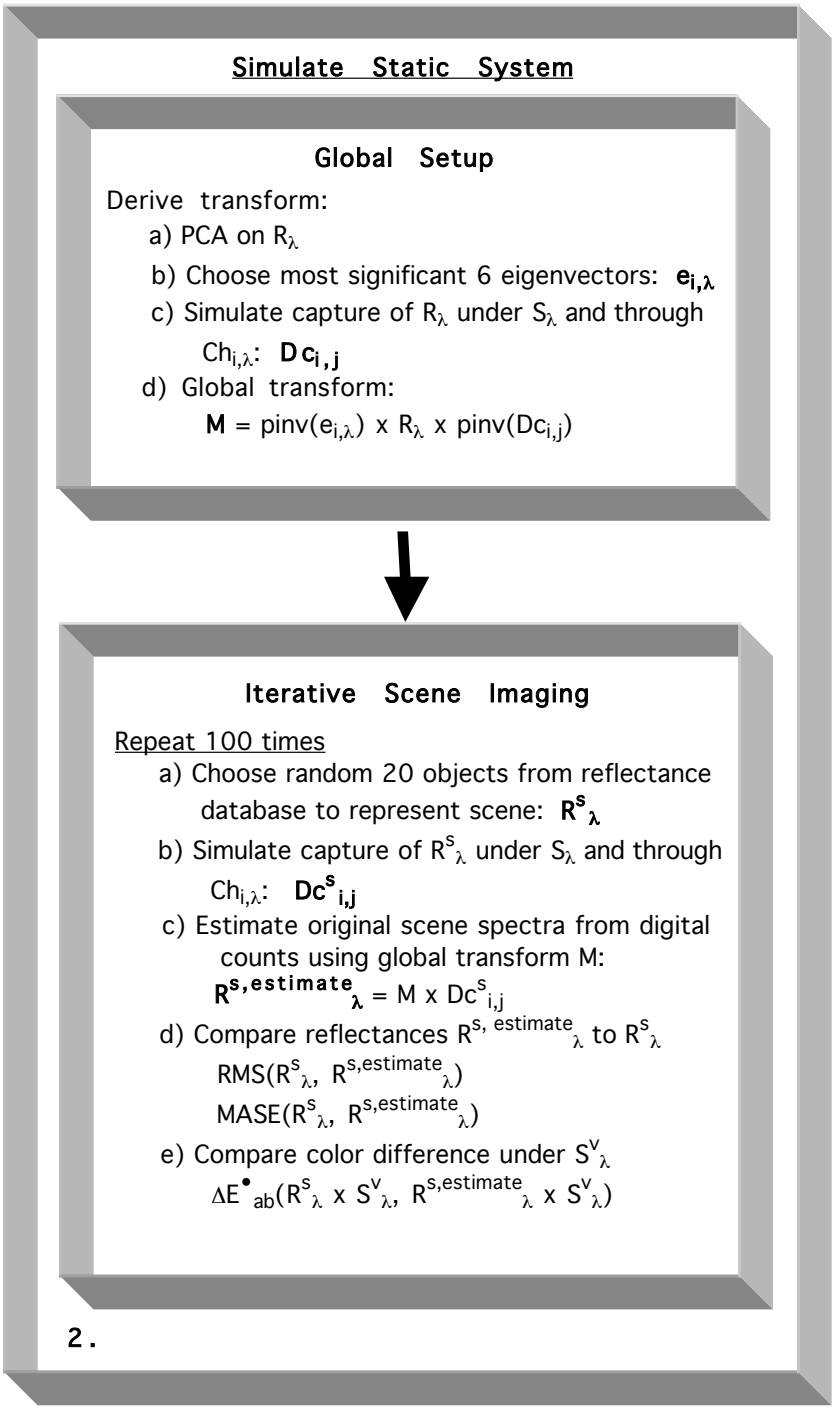
Simulate Static System
Global Setup
Derive transform:
a) PCA on R_λ
b) Choose most significant 6 eigenvectors: $e_{i,\lambda}$
c) Simulate capture of R_λ under S_λ and through $Ch_{i,\lambda}$: $Dc_{i,j}$
d) Global transform:
$M = pinv(e_{i,\lambda}) \times R_\lambda \times pinv(Dc_{i,j})$
Iterative Scene Imaging
Repeat 100 times
a) Choose random 20 objects from reflectance database to represent scene: R^s_λ
b) Simulate capture of R^s_λ under S_λ and through $Ch_{i,\lambda}$: $Dc^s_{i,j}$
c) Estimate original scene spectra from digital counts using global transform M:
$R^{s,estimate}_\lambda = M \times Dc^s_{i,j}$
d) Compare reflectances $R^{s,\,estimate}_\lambda$ to R^s_λ
$RMS(R^s_\lambda, R^{s,estimate}_\lambda)$
$MASE(R^s_\lambda, R^{s,estimate}_\lambda)$
e) Compare color difference under S^v_λ
$\Delta E^*_{ab}(R^s_\lambda \times S^v_\lambda, R^{s,estimate}_\lambda \times S^v_\lambda)$
2.

Figure 8

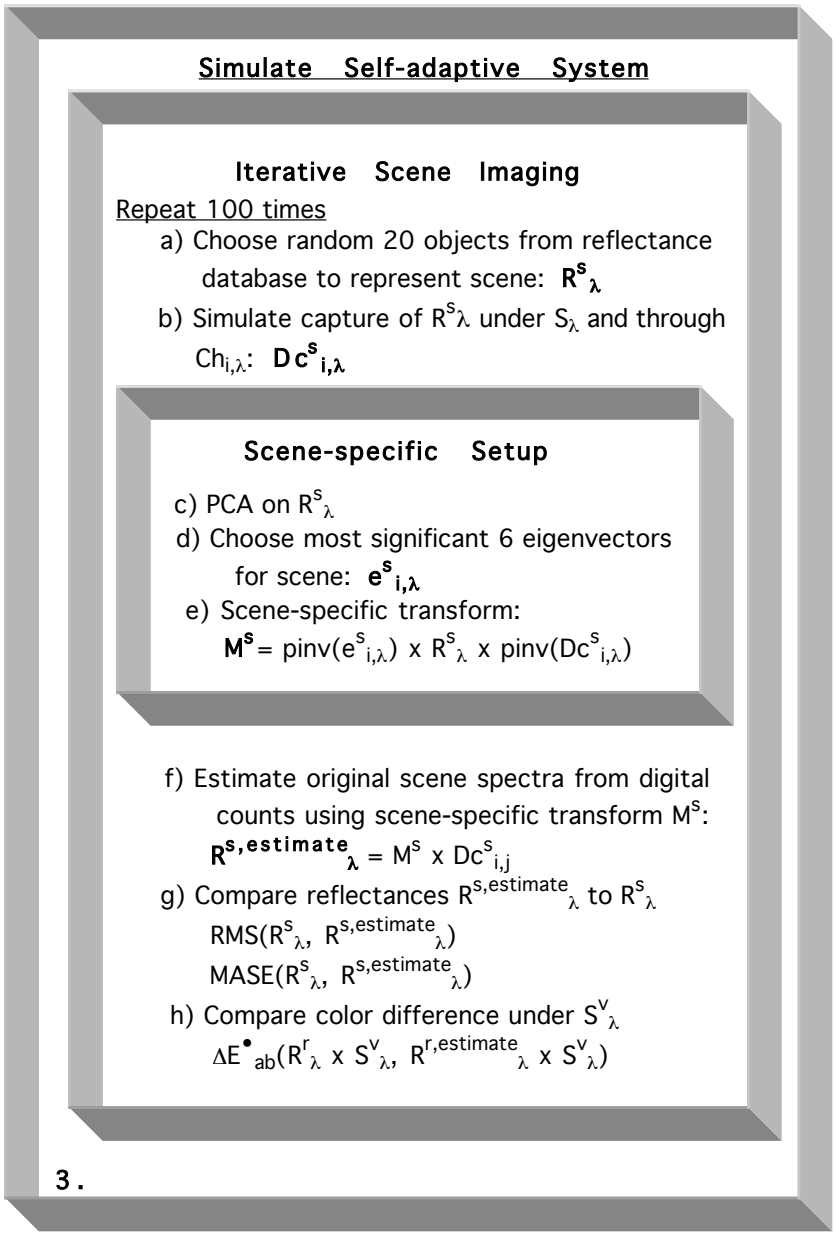
Simulate Self-adaptive System
Iterative Scene Imaging
Repeat 100 times
a) Choose random 20 objects from reflectance database to represent scene: R^s_λ
b) Simulate capture of $R^s\lambda$ under S_λ and through $Ch_{i,\lambda}$: $Dc^s_{i,\lambda}$
Scene-specific Setup
c) PCA on R^s_λ
d) Choose most significant 6 eigenvectors for scene: $e^s_{i,\lambda}$
e) Scene-specific transform: $M^s = pinv(e^s_{i,\lambda}) \times R^s_\lambda \times pinv(Dc^s_{i,\lambda})$
f) Estimate original scene spectra from digital counts using scene-specific transform M^s: $R^{s,estimate}_\lambda = M^s \times Dc^s_{i,j}$
g) Compare reflectances $R^{s,estimate}_\lambda$ to R^s_λ
$RMS(R^s_\lambda, R^{s,estimate}_\lambda)$
$MASE(R^s_\lambda, R^{s,estimate}_\lambda)$
h) Compare color difference under S^v_λ
$\Delta E^*_{ab}(R^r_\lambda \times S^v_\lambda, R^{r,estimate}_\lambda \times S^v_\lambda)$
3.

Figure 9

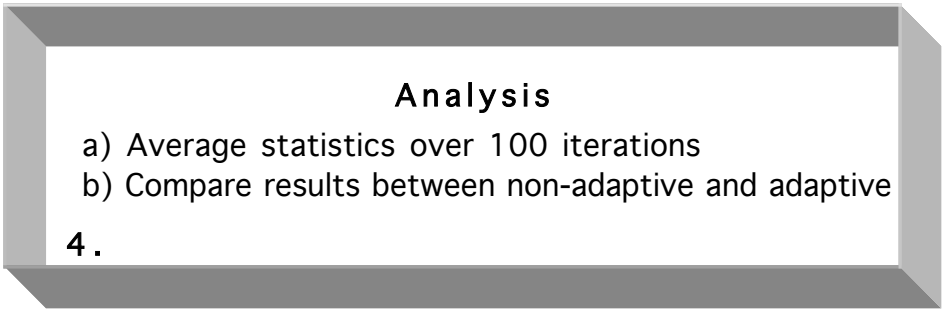
Analysis
a) Average statistics over 100 iterations
b) Compare results between non-adaptive and adaptive
4.

Figure 10

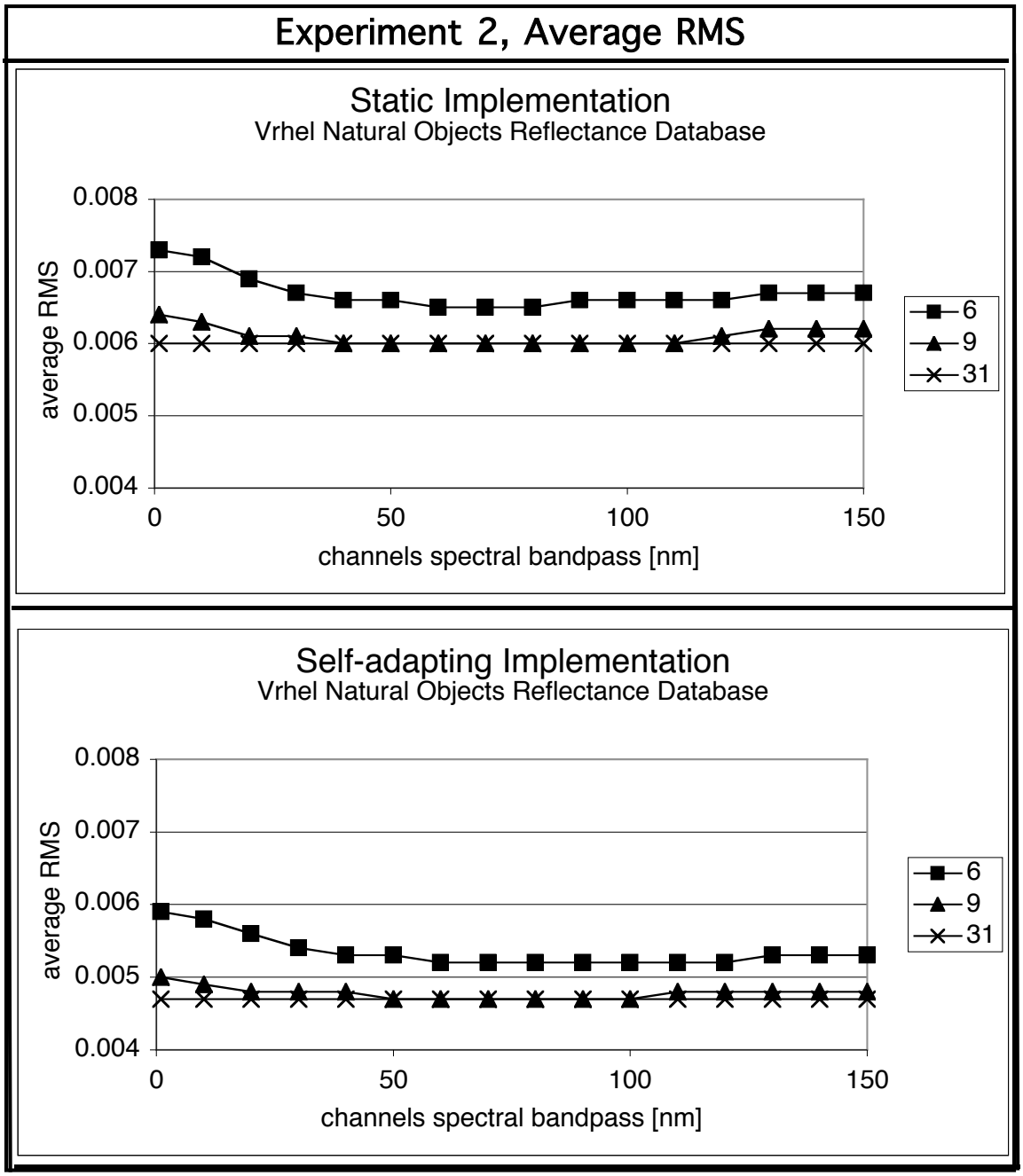
Experiment 2, Average RMS
Static Implementation
Vrhel Natural Objects Reflectance Database
average RMS
0.008
0.007
0.006
0.005
0.004
0
50
100
150
channels spectral bandpass [nm]
6
9
31
Self-adapting Implementation
Vrhel Natural Objects Reflectance Database
average RMS
0.008
0.007
0.006
0.005
0.004
0
50
100
150
channels spectral bandpass [nm]
6
9
31

Figure 11

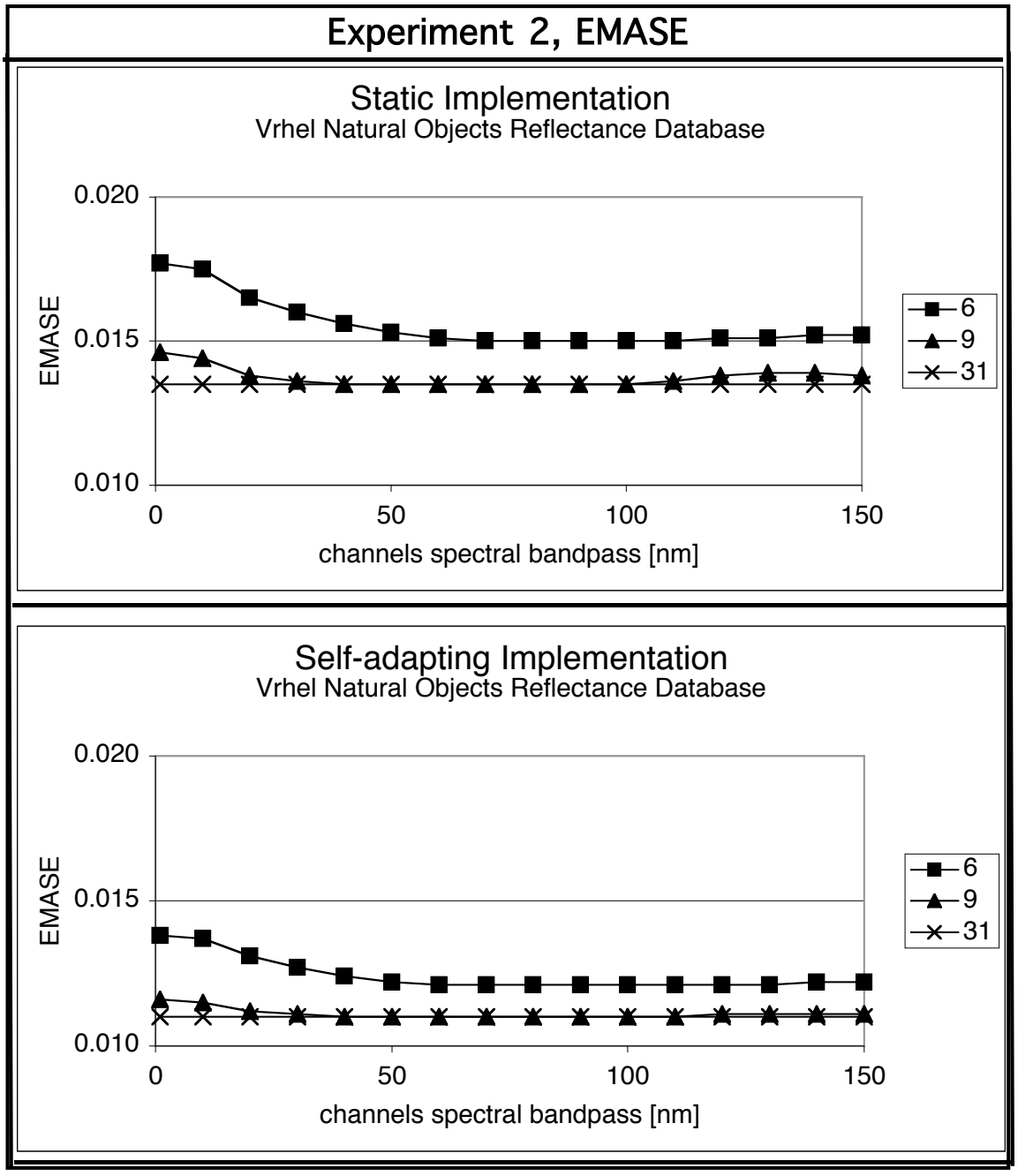
Experiment 2, EMASE
Static Implementation
Vrhel Natural Objects Reflectance Database
EMASE
0.020
0.015
0.010
0
50
100
150
channels spectral bandpass [nm]
6
9
31
Self-adapting Implementation
Vrhel Natural Objects Reflectance Database
EMASE
0.020
0.015
0.010
0
50
100
150
channels spectral bandpass [nm]
6
9
31

Figure 12

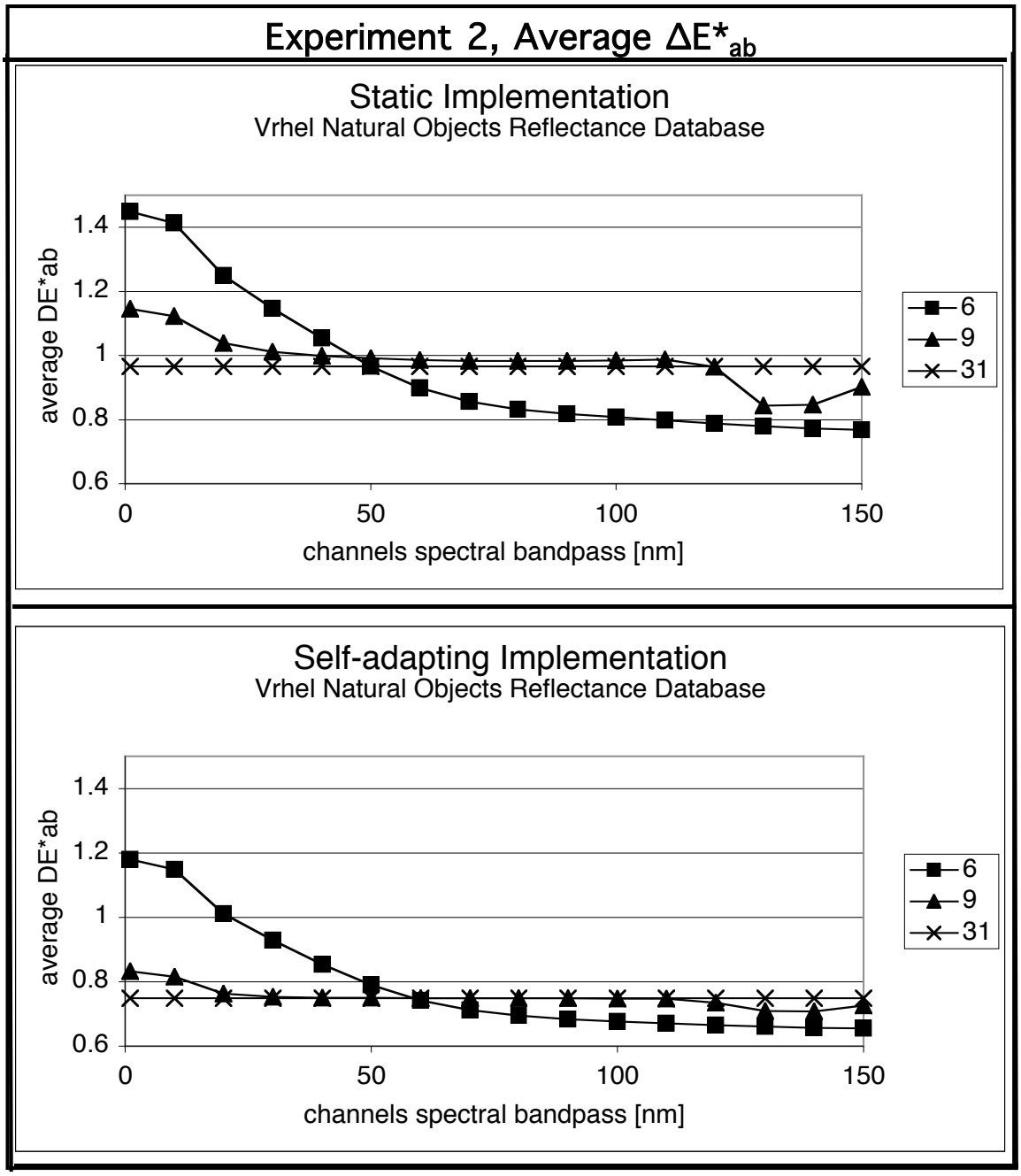
Experiment 2, Average ΔE*ab
Static Implementation
Vrhel Natural Objects Reflectance Database
average DE*ab
1.4
1.2
1
0.8
0.6
0
50
100
150
channels spectral bandpass [nm]
6
9
31
Self-adapting Implementation
Vrhel Natural Objects Reflectance Database
average DE*ab
1.4
1.2
1
0.8
0.6
0
50
100
150
channels spectral bandpass [nm]
6
9
31

Figure 13

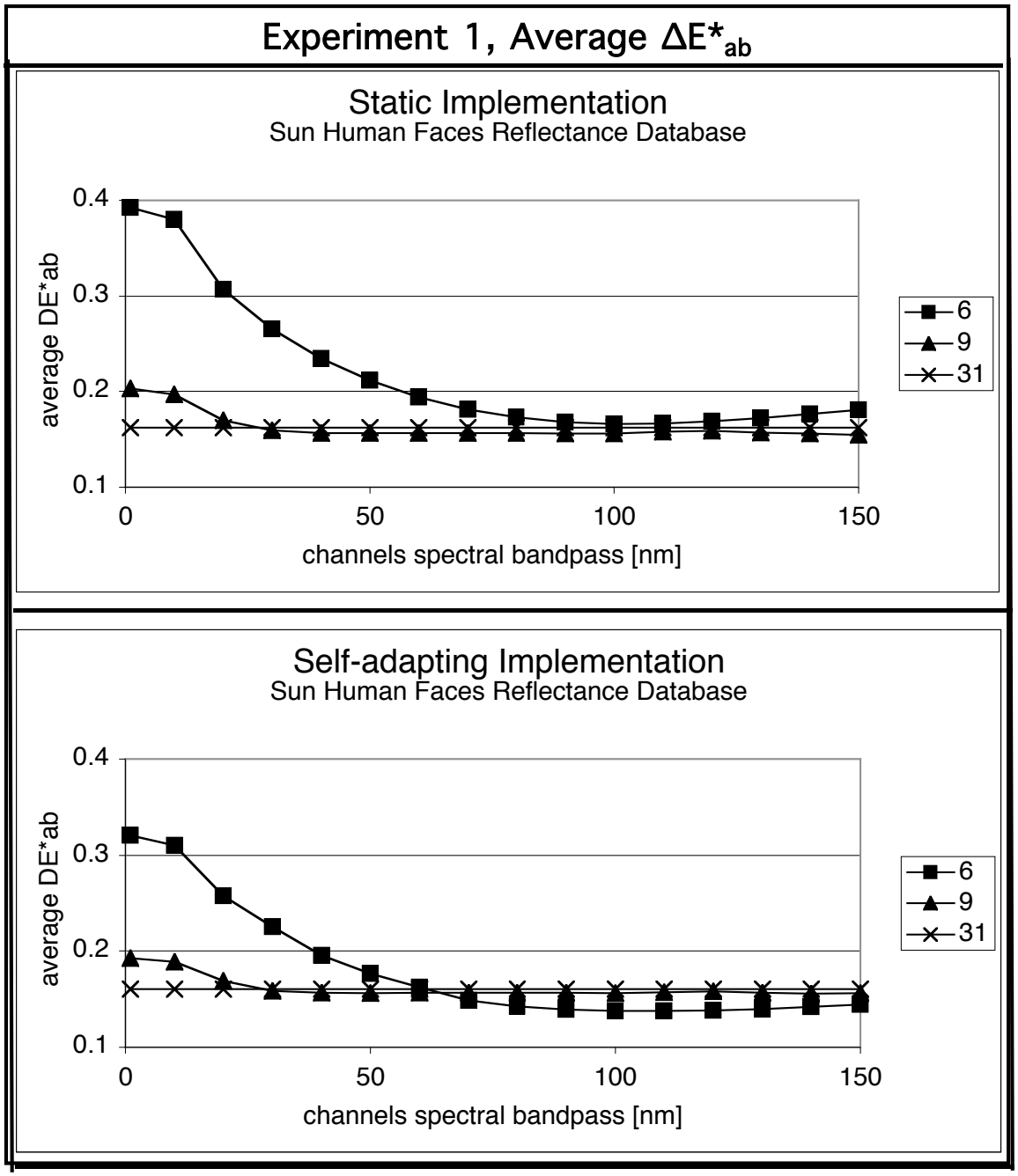
Experiment 1, Average ΔE*ab
Static Implementation
Sun Human Faces Reflectance Database
average DE*ab
0.4
0.3
0.2
0.1
0
50
100
150
channels spectral bandpass [nm]
6
9
31
Self-adapting Implementation
Sun Human Faces Reflectance Database
average DE*ab
0.4
0.3
0.2
0.1
0
50
100
150
channels spectral bandpass [nm]
6
9
31

Figure 14

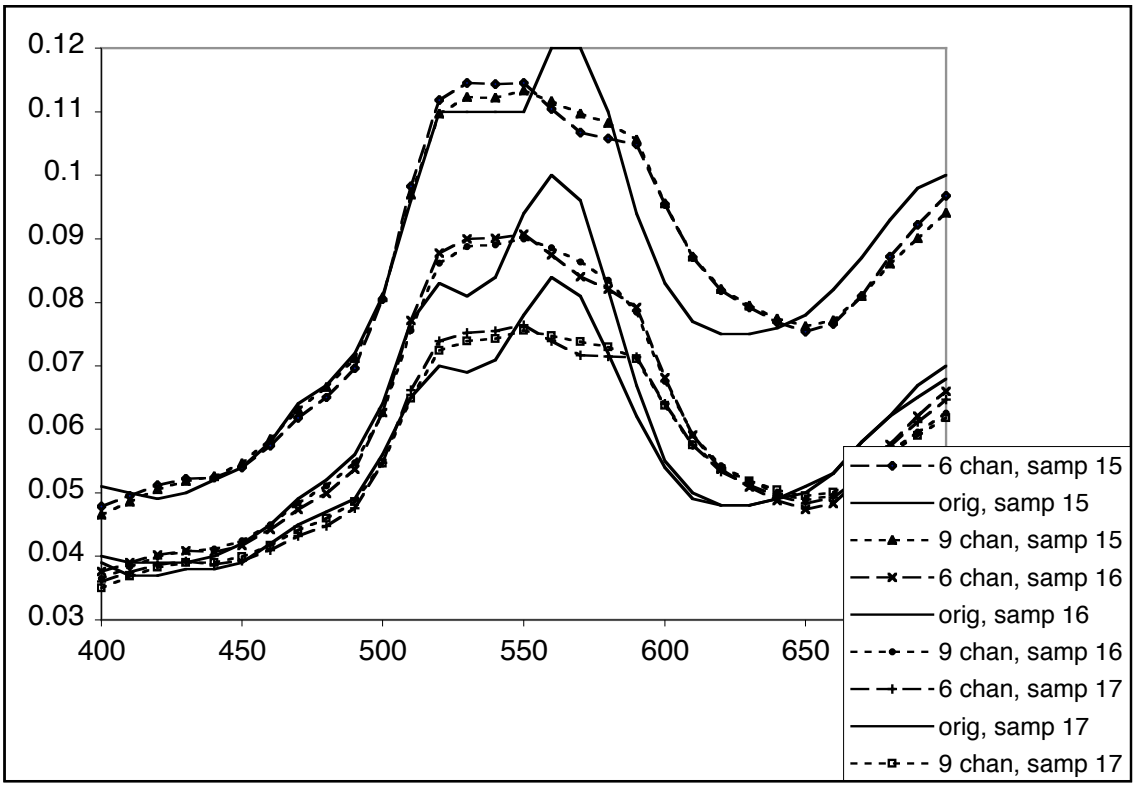
0.12
0.11
0.1
0.09
0.08
0.07
0.06
0.05
0.04
0.03
400
450
500
550
600
650
6 chan, samp 15
orig, samp 15
9 chan, samp 15
6 chan, samp 16
orig, samp 16
9 chan, samp 16
6 chan, samp 17
orig, samp 17
9 chan, samp 17

Figure 15

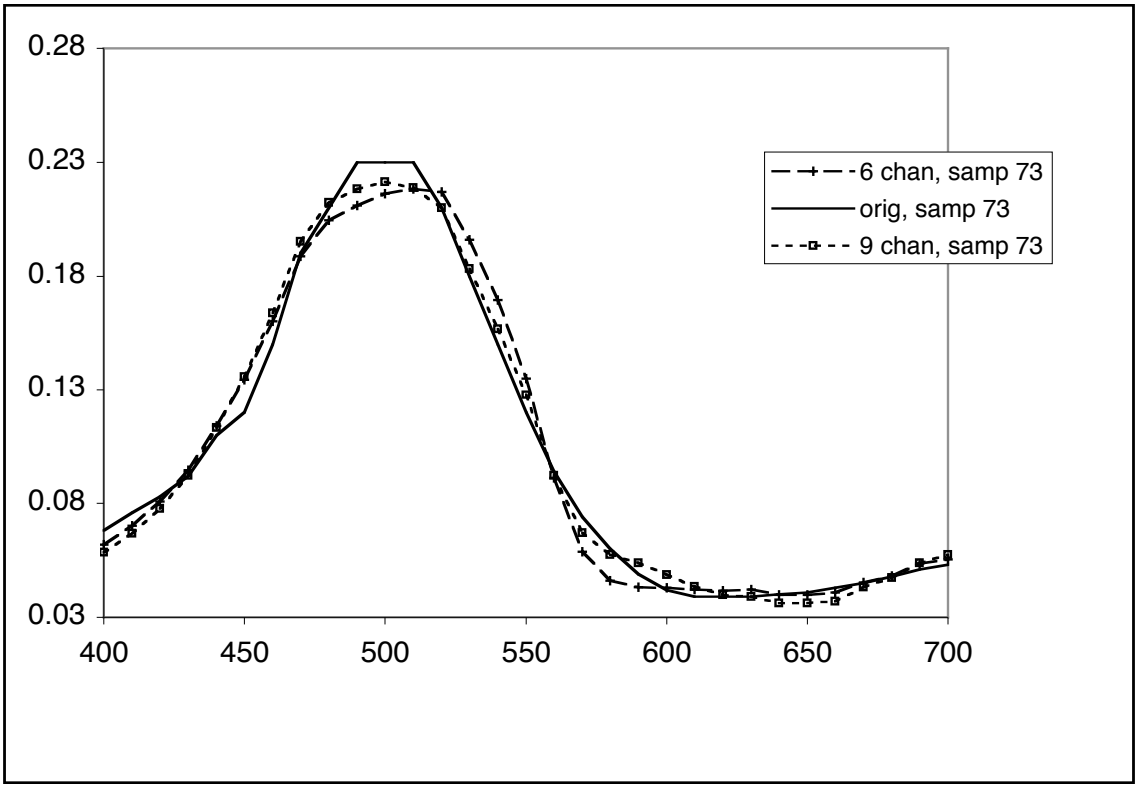
0.28
0.23
0.18
0.13
0.08
0.03
400
450
500
550
600
650
700
6 chan, samp 73
orig, samp 73
9 chan, samp 73

Figure 16

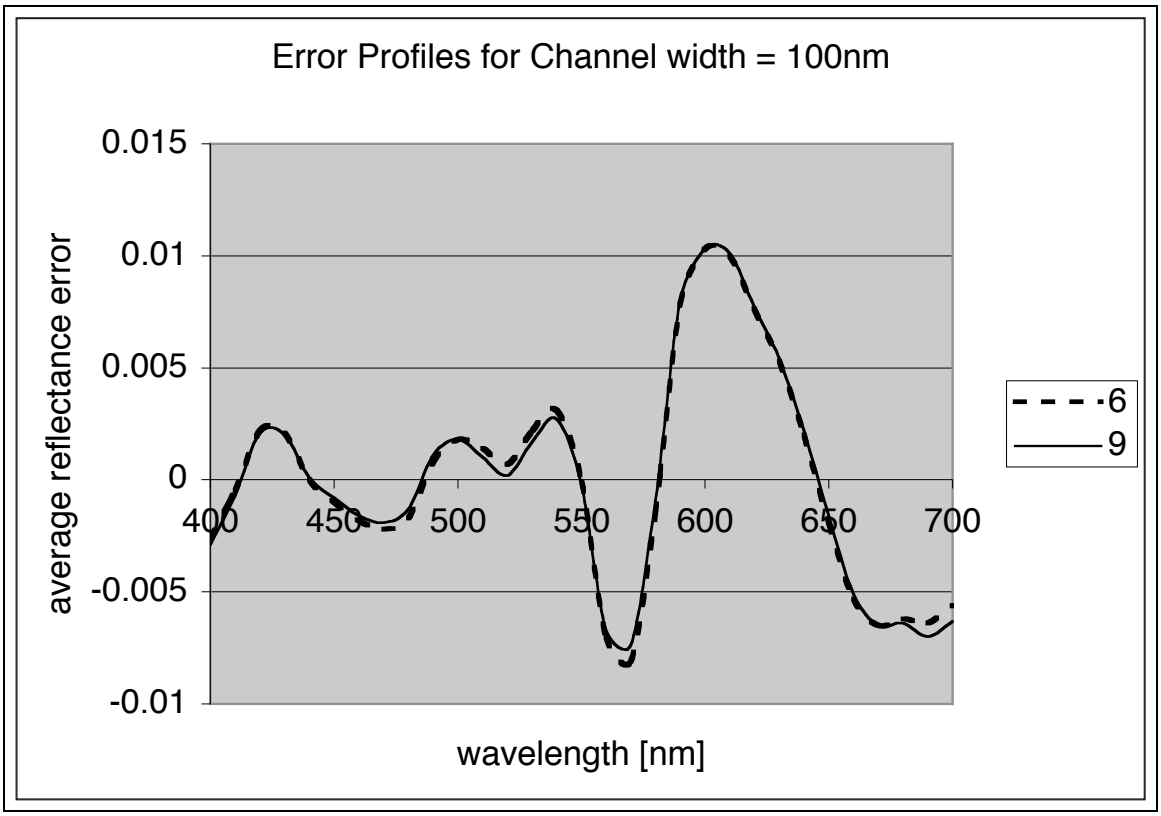
Error Profiles for Channel width = 100nm
0.015
0.01
0.005
0
-0.005
-0.01
average reflectance error
400
450
500
550
600
650
700
wavelength [nm]
6
9

Figure 17

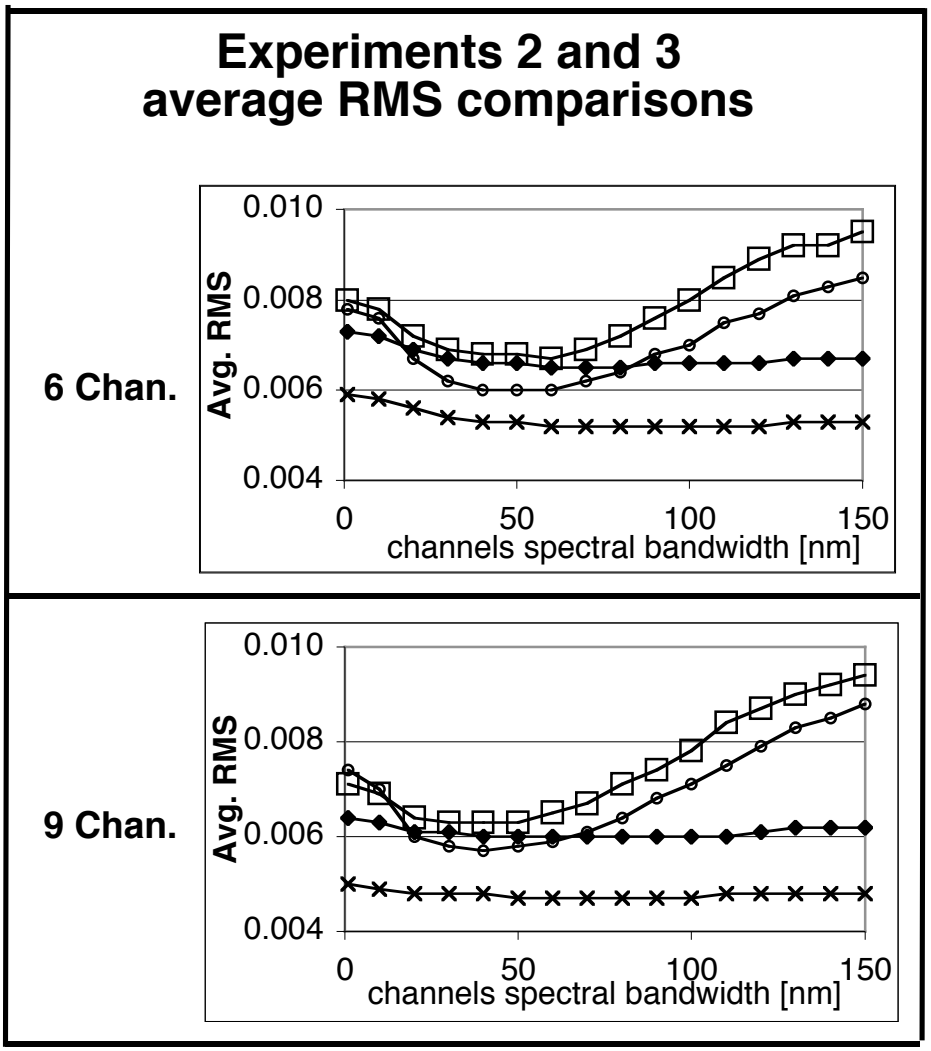
Experiments 2 and 3
average RMS comparisons
6 Chan.
Avg. RMS
0.010
0.008
0.006
0.004
0
50
100
150
channels spectral bandwidth [nm]
9 Chan.
Avg. RMS
0.010
0.008
0.006
0.004
0
50
100
150
channels spectral bandwidth [nm]

Figure 18

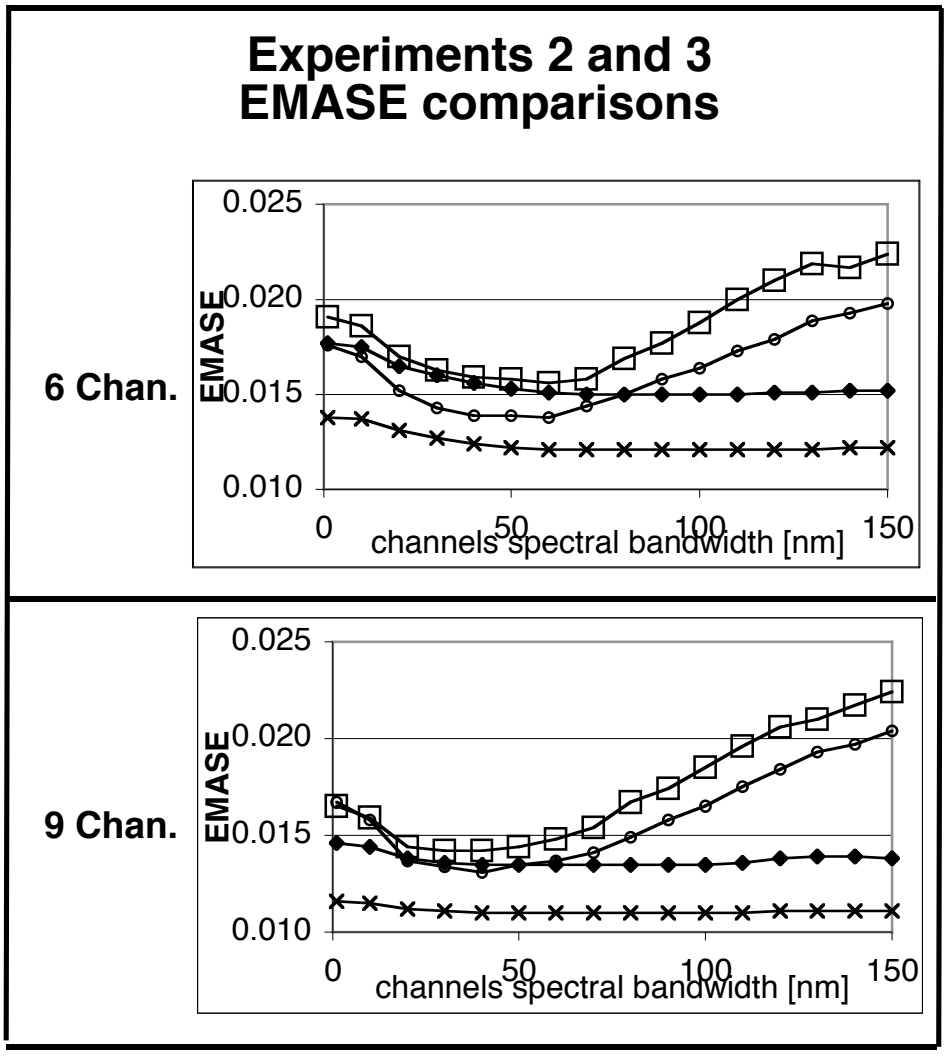
Experiments 2 and 3
EMASE comparisons
6 Chan.
EMASE
0.025
0.020
0.015
0.010
0
50
100
150
channels spectral bandwidth [nm]
9 Chan.
EMASE
0.025
0.020
0.015
0.010
0
50
100
150
channels spectral bandwidth [nm]

Figure 19

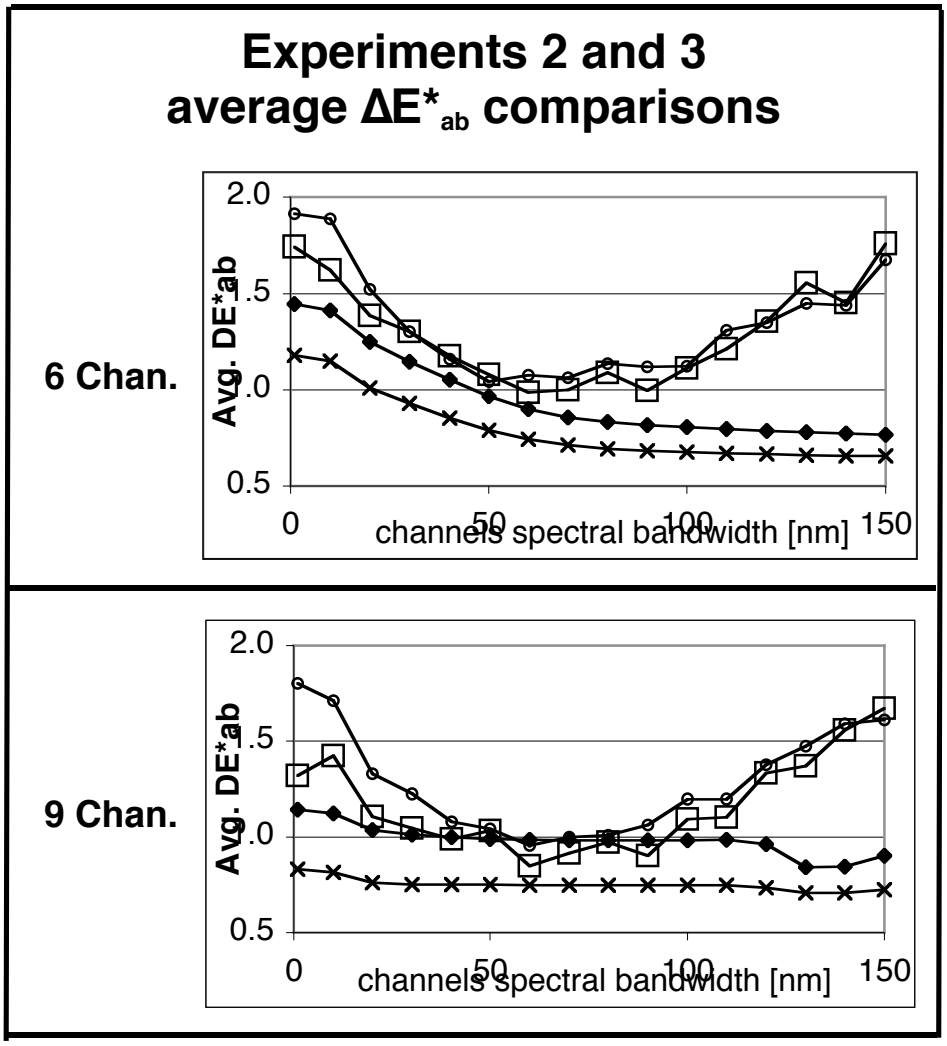
Experiments 2 and 3
average ΔE*ab comparisons
6 Chan.
Avg. DE*ab
2.0
1.5
1.0
0.5
0
50
100
150
channels spectral bandwidth [nm]
9 Chan.
Avg. DE*ab
2.0
1.5
1.0
0.5
0
50
100
150
channels spectral bandwidth [nm]

Figure 20